Molecular Vision 2019; 25:502-516 <http://www.molvis.org/molvis/v25/502>
Received 1 May 2019 | Accepted 19 September 2019 | Published 21 September 2019

Density of PAS positive patterns in uveal melanoma: Correlation with vasculogenic mimicry, gene expression class, BAP-1 expression, macrophage infiltration, and risk for metastasis

Gustav Stålhammar,[1,2,3] Thonnie Rose O. See,[3] Stephen S. Phillips,[3] Hans E. Grossniklaus[3]

[1]Ophthalmic Pathology and Oncology Service, St. Erik Eye Hospital, Stockholm, Sweden; [2]Department of Clinical Neuroscience, Karolinska Institutet, Stockholm, Sweden; [3]Departments of Ophthalmology and Pathology, Emory University School of Medicine, Atlanta, GA

Purpose: Periodic acid-Schiff (PAS) positive patterns of vasculogenic mimicry (VM) have been associated with poor prognosis in uveal melanoma (UM). We examined these patterns with digital image analysis and transmission electron microscopy, and correlated them with BAP-1 expression, gene expression class, macrophage infiltration, and metastatic disease in full tumor cross-sections and intratumor regions.

Methods: Thirty-two enucleated eyes with UM were stained immunohistochemically (BAP-1, laminin, CD31, and CD68) and with PAS without hematoxylin counterstain. Retrospective data on gene expression class and patient survival were retrieved. Tumor sections were digitally scanned and analyzed with the QuPath Bioimage analysis software, and imaged with transmission electron microscopy.

Results: The mean area proportion covered by CD31, laminin, and PAS positive patterns in tumor cross-sections was 0.9% (SD 0.6), 3.0% (SD 1.9), and 8.4% (SD 5.9), respectively. PAS density was statistically significantly greater in tumors with gene expression class 2 (p=0.02). The cumulative 5-year metastasis-free survival decreased for each quartile of increased PAS density (1.0, 0.75, 0.40, and 0.17, p=0.004). Forty percent of the tumors had heterogeneous BAP-1 expression. Intratumor regions with low BAP-1 expression were more likely to harbor VM (p<0.0001), and had statistically significantly greater PAS density (p<0.0001) and number of CD68 positive cells (p=0.01).

Conclusions: PAS positive patterns in UM are composed of a mixture of blood vessels and extracellular matrix (ECM), including VM. Increased density of PAS positive patterns correlated with gene expression class and metastasis, and colocated to tumor regions with macrophage infiltration and low BAP-1 expression.

Uveal melanoma (UM) is the most common primary intraocular malignancy in adults. Due to the absence of lymphatic drainage of the ocular interior, tumor spread occurs almost exclusively by the hematogenous route, ultimately leading to the death of approximately 40% of patients [1]. Once a metastasis is detected, median survival is less than 6 months with no effective treatment available [2,3].

The presence of an alveolar histological pattern in rapidly growing UM was first described by Fuchs in 1882 [4,5]. These patterns, appearing as loops, arcs, and lines in stains with periodic acid-Schiff (PAS), were later characterized as patterned extracellular matrix (ECM), or tubules without endothelial lining that connect to more mature vessels [6,7]. The term vasculogenic mimicry (VM) was coined by Maniotis et al. in 1999, to describe the de novo formation of these patterns by aggressive UM [7]. Melanoma cells have been found to actively remodel the uveal ECM by expression of type VI collagen and other matrix components, serving as a scaffold for vascular networks [8].

The correlation between VM, gene expression class, and increased rates of metastasis in UM is well documented [4,9-12]. Further, the density of microvessels has been shown to be an independent contributor to melanoma-specific mortality [13,14]. After adjustment for density, the independent relationship between VM and poor survival disappeared [14].

Previous studies of VM in UM relied on manual assessments of the presence or absence of up to nine qualitatively distinct patterns in PAS stained pathology slides [4,6,7,14]. In studies of vascular density, pathology slides were stained with immunohistochemical markers for endothelium (CD31, CD34, and factor VIII-related antigen), angiogenesis-related endothelium (CD105), or proteins in the extracellular matrix (ECM; collagen type IV, collagen type VI, and α-smooth muscle Actin) [8,13,15-17]. In two of these studies, the number of vessels seen within three high-power fields was counted manually, with good intraobserver, interobserver, and interreagent agreement reported [13,17]. An association between tumor-infiltrating macrophages and vascular density

Correspondence to: Gustav Stålhammar, Oncology and Pathology Service, St. Erik Eye Hospital, Polhemsgatan 50, 112 82, Stockholm, Sweden; Phone: +46 8 672 30 00; FAX: 00468 672 33 75; email: gustav.stalhammar@ki.se

has been noted [18,19]. In turn, loss of nuclear BRCA1 associated protein 1 (BAP-1) expression correlates with increased risk for metastasis, and has been associated with increased numbers of T cells and macrophages in disomy 3 tumors [20-23].

However, limited insight has been offered into the interrelations of different constituents of the PAS positive patterns and their independent prognostic significance as defined by objective means. The proportions of the subcomponents of these patterns, including blood vessels and basal laminae, have not been quantified and related to each other. PAS density has not been compared to gene expression class, and neither PAS density nor VM to tumor cell BAP-1 expression. Furthermore, the level of intratumor heterogeneity in immunohistochemical markers has not been quantified or compared, let alone by algorithms with minimized subjective assessment.

METHODS

Patients and samples: The study adhered to the tenets of the Declaration of Helsinki. The study protocols adhered to the tenets of the Declaration of Helsinki and the ARVO statement on human subjects. The protocol for the collection of specimens and data was approved by the Emory Institutional Review Board, Emory University (Atlanta, GA; October 10 2018, AM1_IRB00105948). Power analysis was used to determine the sample size in the present study. With a power of 0.80 (given a two-sided α of 0.05), a total sample size of 32 patients would be required to detect a difference in survival probability of 0.46 between the first two and last two quartiles, which has been published previously in a study of microvascular density in UM [13]. Enucleated formalin fixed paraffin embedded (FFPE) eyes with UM were then sampled from patients who had undergone enucleation at the Emory Eye Center from December 17, 2009, through November 22, 2017. Inclusion criteria were histologically proven UM, and availability of gene expression classification and survival data. Exclusion criteria were previous history of brachytherapy, proton beam irradiation, external radiation, anti-VEGF treatment, or FFPE block unavailable, or insufficient or too necrotic tumor tissue for BAP-1 immunohistochemistry. After the medical records were reviewed, 56 enucleated eyes met the inclusion criteria, 26 of which were excluded due to the following: brachytherapy before enucleation (n=2), FFPE block unavailable (n=22), specimen with 100% necrotic tumor (n=1), and insufficient specimen for BAP-1 immunohistochemistry (n=1).

Staining and digital scanning: Each FFPE eye was cut into multiple 4-µm sections in the area of the central tumor cross-section. One section per tumor was then stained with PAS without hematoxylin counterstain. The other four sections were pretreated in EDTA buffer at pH 9.0 for 20 min, and incubated with mouse monoclonal antibodies against BAP-1 (sc-28383; Santa Cruz Biotechnology, Dallas, TX) at dilution 1:40, against CD31 (ab134168; Abcam PLC, Cambridge, UK) at dilution 1:400, against laminin (m063801–2; Dako, Agilent Technologies, Santa Clara, CA) at dilution 1:20, and against CD68 (M087601–2, Dako) at dilution 1:200, according to the manufacturers' instructions. A red chromogen was used. Finally, the slides were counterstained with hematoxylin and rinsed with deionized water. The deparaffinization, pretreatment, primary staining, secondary staining and counterstaining steps were run in a Bond III automated immunohistochemistry (IHC) and in situ hybridization (ISH) stainer (Leica, Wetzlar, Germany). The dilutions were gradually titrated until optimal staining was achieved, according to manual control. All slides were then digitally scanned at 40X, using a Nano Zoomer 2.0 HT (Hamamatsu Photonics K.K., Hamamatsu, Japan) at the Winship Research Pathology Core Laboratory, Winship Cancer institute of Emory University (Atlanta, GA).

Digital pattern recognition: The digital image analysis software used was QuPath Bioimage analysis v. 0.1.2, which is open source software for digital pathology and whole slide image analysis developed at Northern Ireland Molecular Pathology Laboratory, Queen's University (Belfast, Northern Ireland, UK) [24]. The software was run on a standard off-the-shelf laptop computer (Apple, Inc. Cupertino, CA).

The density of the PAS-, laminin-, and CD31-stained structures and cells was determined with the following method: After calibration of the positive stain vector (a PAS, laminin, or CD31 positive structure or cell) and the negative stain vector (tissue not stained by PAS, laminin, or CD31) in each tumor, a polygon region of interest was drawn along the margins of the tumor. Thus, all non-tumor tissues were excluded, including the sclera, Bruch's membrane, the retina, and the vitreous. Tumor areas with intense inflammation, abundant pigmentation, fibrosis, bleeding, necrosis, tissue folds, or poor fixation were also excluded. The "positive pixel count" function was then run with the settings described below. As we strived to maximize ease of use, we wanted to limit the manual inputs required, and thus, elected to not use any of the more advanced features of the software. PAS, laminin, and CD31 density was defined as the number of PAS, laminin, or CD31 positive pixels divided by the total number of pixels in the analyzed tumor area, expressed as a percentage (Figure 1).

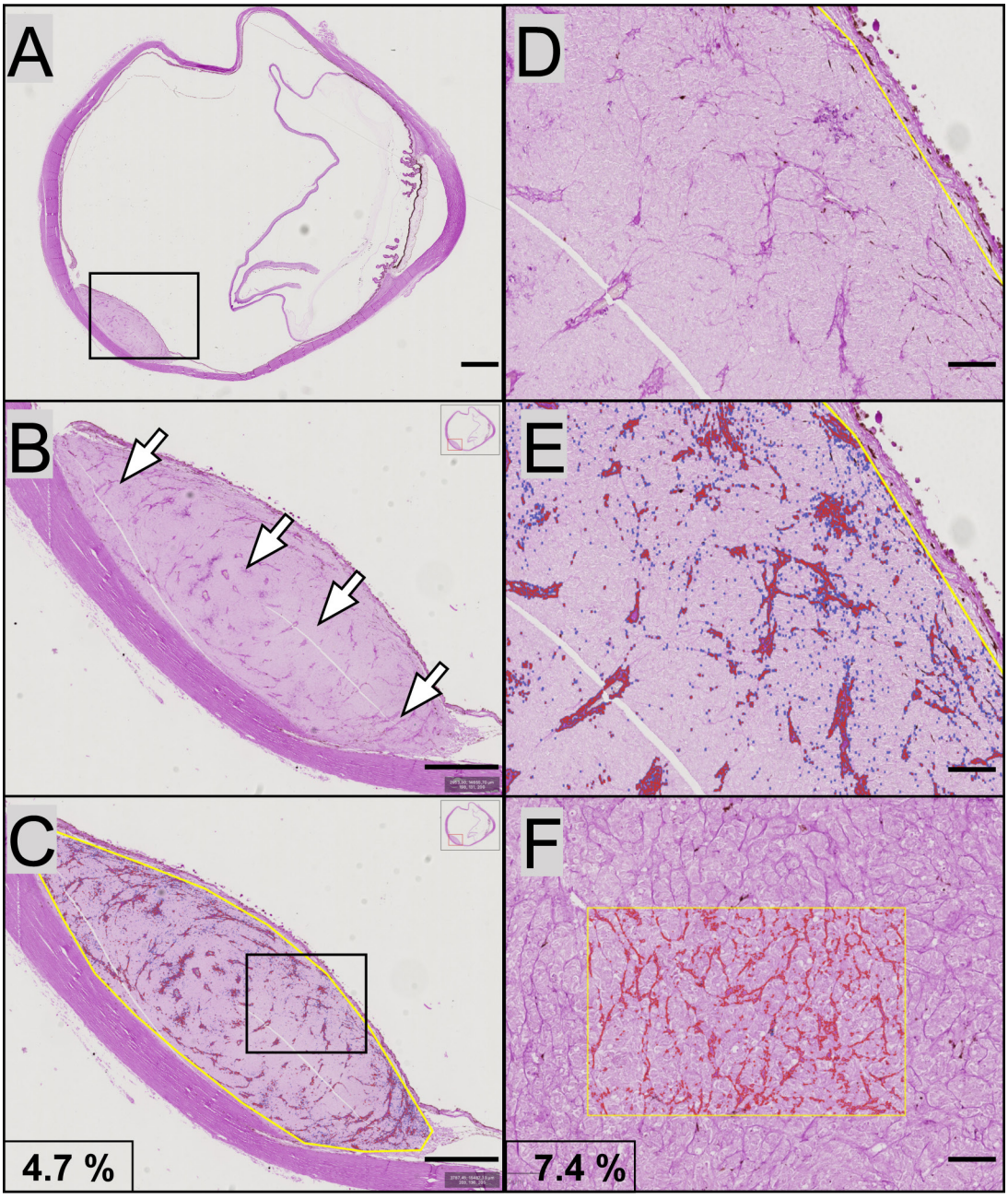

Figure 1. Examples of digital pattern recognition of PAS positive structures. **A**: A glass slide with a dome-shaped uveal melanoma in the posterior aspect of the eye was digitally scanned and imported to the QuPath Bioimage analysis software. **B**: In higher magnification, multiple periodic acid-Schiff (PAS) positive structures can be identified in the interior of the tumor (arrows). **C**: A region of interest is outlined along the tumor's margins (yellow line). Within this region of interest, the software automatically identified PAS positive patterns (marked red). As indicated, the PAS density in this full tumor cross-section was 4.7% (PAS positive pixels divided by the total number of pixels). **D**: In even higher magnification of the same tumor, vessels are easier to identify. **E**: The digital pattern recognition marked all PAS positive structures red. **F**: In a second tumor, patterns of vasculogenic mimicry (VM) including closed loops and networks can be identified. In the square region of interest, the digital pattern recognition of the VM is visualized in red. The PAS density in the square region was 7.4%. Scale bars, a: 2 mm. b, c: 1 mm. d, e and f: 200 µm.

The following settings were used for all tumors:: 1) The downsample factor was set to 4, a compromise between retaining data in the image files and the time required for processing. In short, this is the factor of the reduction of the original file size before analysis. A factor of 5 or 6 would have reduced the file size to one fifth or one sixth, respectively.

2) Gaussian sigma was set to 0.5 µm. Higher values give a smoother but less detailed result, with a risk of finer details being excluded.

3) The PAS, laminin, and CD31 detection threshold was set to 0.30 optical density units, and the hematoxylin threshold to 0.01 optical density units.

Other than the initial drawing of regions of interest, there was no further human intervention with the operation of the software or its results. All operations were performed blinded to all patient data (patient identity, metastatic and survival outcomes, BAP-1 expression, gene expression class, and VM).

In addition to measurements of full tumor cross-sections for intratumor comparisons, we subdivided tumors into multiple regions for measurement on the intratumor level. Circular sections with a diameter of 2.0 mm were used for digital pattern recognition of PAS density as described above, and for manual assessment of the presence of VM, BAP-1, and CD68 expression in corresponding intratumor regions. For measurement of intratumor heterogeneity in PAS density, each tumor was further subdivided into circular sections with a diameter of 0.5 mm for increased resolution.

Vasculogenic mimicry: Patterns of microvascular loops and networks were assessed independently by two pathologists under a light microscope with a green narrow band pass filter, according to the method described by Folberg et al. [11]. The pathologists were blinded to all patient data, as described above. Nine patterns were evaluated: normal (within the portion of the tumor beneath Bruch's membrane), silent, straight, parallel, parallel with crosslinks, arcs, arcs with branches, closed loops, and networks. Any presence of one or several of the patterns within any given tumor was recorded. Discrepancies in assessments were solved by a consensus discussion, in which the two observers reevaluated cases with dissimilarly recorded patterns under a multihead microscope. The specific tumor areas containing these patterns were examined and discussed until consensus about their classification was reached.

Gene expression classification: Tumor tissue samples had been obtained from freshly enucleated eyes with fine needle aspiration. The contents of the needle hub were then transferred into one of two RNase-free cryovials. Using the same needle, extraction buffer from the second cryovial was aspirated and expelled into the first. This vial was then placed in a specimen bag, immediately frozen to −80 °C, and shipped on dry ice for gene expression classification based on 12 discriminating genes (*HTR2B* [Gene ID 3357, OMIM 601122], *ECM1* [Gene ID 1893, OMIM 602201], *RAB31* [Gene ID 11031, OMIM 605694], *CDH1* [Gene ID 999, OMIM 192090], *FXR1* [Gene ID 8087, OMIM 600819], *LTA4H* [Gene ID 4048, OMIM 151570], *EIF1B* [Gene ID 10289], *ID2* [Gene ID 3398, OMIM 600386], *ROBO1* [Gene ID 6091, OMIM 602430], *LMCD1* [Gene ID 29995, OMIM 604859], *SATB1* [Gene ID 6304, OMIM 602075], and *MTUS1* [Gene ID 57509, OMIM 609589]) and three control genes (*MRPS21* [Gene ID 54460, OMIM 611984], *RBM23* [Gene ID 55147], and *SAP130* [Gene ID 79595, OMIM 609697]) at a commercial laboratory (Castle Biosciences Inc. Friendswood, TX) [25]. This classification has been proven to accurately discriminate patients who eventually develop metastases [26]. All samples were processed during routine clinical testing for risk prognostication after patient consent was obtained.

Transmission electron microscopy: Three 2 × 2 × 2 mm pieces from one primary tumor tissue were manually dissected, and fixed in 2.5% glutaraldehyde. The tissue pieces were then washed in sodium cacodylate buffer for 15 min and post-fixed in 1.0% osmium tetroxide (OsO_4) for 2 h at room temperature, after which they were rinsed in deionized water. Each piece was sequentially dehydrated in a series of increasing ethanol concentrations (35–100%) and embedded overnight in a 1:1 mixture of propylene oxide and LX112 resin, followed by pure LX112 resin. They were put in a vacuum desiccator for 4 h, and then in a 60 °C oven for 2 days to polymerize. One-micrometer sections were cut with an ultramicrotome, and stained with an aqueous solution of 1% toluidine blue and 1% sodium borate. From areas of interest, additional 70-nm sections were cut and stained with 2% aqueous uranyl acetate and with Reynold's lead citrate. Last, a tungsten-filament transmission electron microscope (JEM-100CX II, JEOL Ltd. Tokyo, Japan) with an attached 16-megapixel digital camera (Scientific Instruments and Applications Inc., Duluth, GA) was used to image the prepared sections at magnifications of 1,400X to 10,000X. Tumor cells were identified by an increased nucleus-to-cytoplasm ratio, presence of large nuclei, nucleoli, premelanosomes, or melanosomes [27].

BAP-1 and CD68 expression: Nuclear BAP-1 reactivity had previously been assessed using a four-point scoring system [20]. Briefly, the tissue sections were screened under low magnification (40X), and the three areas exhibiting the most intense BAP-1 staining selected for grading. Nuclear immunoreactivity was then evaluated in approximately 100 cells in

each area (at 200X). The level of BAP-1 expression was classified as low if <33% of the tumor cell nuclei in the 200X field were positive, and as high if ≥33% were positive. Two independent pathologists performed the manual scoring blinded to all patient data. Discrepancies in assessments were solved with a consensus discussion, in which the two observers reevaluated 100 cells in one or several areas (at 200X) under a multihead microscope until consensus about the classification was reached. For the assessment of the concentration of macrophages and their correlation to BAP-1 expression, VM, and PAS density, the number of CD68 positive cells within each of the circular 2.0 mm diameter intratumor regions was counted manually.

Statistical methods: For analysis of PAS density, the global area percentage of PAS positive pixels was calculated as described above. We also calculated the density of CD31, CD68, and laminin positive pixels and the extent of intratumor heterogeneity, defined as the difference in percentage points between the intratumor regions with the least and most dense vasculature, and in regions defined as the base, center, and apex. Differences with a p value of less than 0.05 were considered statistically significant, all p values being two-sided. The deviation of all counts from normal distribution was statistically significant, when evaluated with the Shapiro–Wilk test ($p<0.05$). For tests of continuous variables between two groups, therefore, we used the Mann–Whitney *U* test, which does not assume normally distributed data. For comparisons among the three groups, we used the Kruskal–Wallis test. For comparisons of PAS density in tumors with and without patterns of VM, of gene expression class 2 versus 1 and with low and high levels of BAP-1 expression, two-by-two tables and Fisher's exact test or likelihood ratios were used. For comparisons of association with metastasis, bivariate logistic regressions, multiple logistic regressions, and multiple Cox proportional hazards regressions were applied, with tumor thickness as a covariate to adjust for the contribution of tumor size to prognosis [28]. Cumulative Kaplan–Meier metastasis-free survival for quartiles of increasing PAS density, as well as for groups separated by the median PAS density, was calculated. Event-free follow-up was defined as the time in months from enucleation to the last occasion metastasis-free patients were seen or in contact alive. All statistical analyses were performed using IBM SPSS statistics version 25 (Armonk, NY).

RESULTS

Descriptive statistics: There were 15 women and 17 men in the cohort, with a mean age at enucleation of 62 years. Thirty (94%) of the tumors engaged the choroid, with seven (22%) and one (3%) tumors also engaging the ciliary body and the iris, respectively. Mean tumor thickness was 8.8 mm and mean diameter 15.5 mm, spanning all four American Joint Committee on Cancer (AJCC) T-categories. Seven (23%) tumors were of gene expression class 1a, eight (25%) of class 1 b, and 15 (47%) of class 2. BAP-1 expression was classified as high in 12 (38%) tumors and as low in 20 (63%) tumors. Metastases were detected in 14 of the 32 patients (44%). The mean event-free follow-up was 28 months (Table 1).

Of the 32 tumors that were assessed for PAS density, we were not able to obtain results from four, due to abundant pigmentation (n=2), widespread necrosis (n=1), and severely dilated vessels with distorted morphology due to strangulation in Bruch's membrane (n=1). The mean tumor area analyzed in each of the remaining 28 tumors was 42 mm^2 (SD 25). The mean area proportion covered by CD31, laminin, and PAS positive blood vessel endothelium was 0.9% (SD 0.6), fivefold less than the area proportion covered by CD31, laminin, and PAS positive basal laminae of VM and blood vessels combined (3.0%, SD 1.9). The mean area proportion of CD31, laminin, and PAS positive ECM was 5.4% (SD 3.5). The mean area proportion covered by all PAS positive structures was 8.4% (SD 5.9, Figure 2A,B).

PAS density versus vasculogenic mimicry: Of the 28 tumors, the normal pattern of VM was identified in 26, silent pattern in four, straight pattern in two, parallel pattern in five, parallel with crosslinks pattern in nine, arcs in five, arcs with branching in ten, closed loops in 15, and networks in 12 tumors. In a multiple Cox proportional hazards regression with tumor thickness as a covariate to the presence of networks, closed loops, or arcs with branching, or any combination, the time-dependent hazard for metastasis was statistically significantly increased for patients who had tumors with these patterns (hazard pattern versus no pattern=9.6, 95% confidence interval [CI] 1.2–77.9, p=0.03). PAS density was statistically significantly greater in tumors with the presence of these patterns (Mann–Whitney *U* test p=0.04, Figure 2C). The presence of these patterns was also associated with a global PAS density greater than the median (Fisher's exact p=0.02). When adjusted for global PAS density, the prognostic significance of VM disappeared (multiple Cox proportional hazards regression, pattern versus no pattern with PAS density less or greater than the median as covariate=0.7, 95% CI 0.5–8.4, p=0.8).

Transmission electron microscopy: In transmission electron microscopy, the difference between blood vessels, VM, and collagenous strands could be appreciated. As suggested with the immunohistochemical stains, it was deemed that the PAS positive patterns were composed of a mix of 1) dense strands

of ECM laid down by fibroblasts and macrophages, 2) extracellular debris, 3) thin channels with potential lumens (VM) that in most areas were lined by tumor cells identifiable by their large nuclei with nucleoli, coarse chromatin, and cytoplasmic melanosomes, 4) basal laminae, and 5) mature blood vessels with endothelial lining. Furthermore, the potential lumens of VM could be tracked to larger fluid-filled sinuses with open lumen and a diameter of approximately 5–10 µm (Figure 3).

PAS density versus gene expression classification: In a multiple Cox proportional hazards regression with gene

Table 1. Characteristics of patients and tumors included in this study.

n =	**32**
Mean age at enucleation, years (min—max)	62 (24–92)
Sex, n (%)	
Female	15 (47)
Male	17 (53)
Tumor location, n (%)	
Choroid only	22 (69)
Choroid and ciliary body	7 (22)
Choroid, ciliary body and iris	1 (3)
Iris only, or ciliary body and iris	2 (6)
Cell type, n (%)	
Spindle	2 (6)
Epitheloid	4 (13)
Mixed	26 (81)
Mean tumor thickness, mm (min—max)	8.8 (1.1–17.4)
Mean tumor diameter, mm (min—max)	15.5 (4.8–22.5)
Previous brachytherapy, n (%)	
No	32 (100)
Yes	0 (0)
AJCC T-category, n (%)	
1	2 (6)
2	6 (19)
3	16 (50)
4	8 (25)
Gene expression class, n (%)	
1a	7 (23)
1b	8 (25)
2	15 (47)
Na	2 (6)
Manual BAP1 classification, n (%)	
High	12 (38)
Low	20 (63)
Follow-up months, mean (SD, min—max)	28 (20, 2–56)
Metastasis, n (%)	
No	18 (56%)
Yes	14 (44%)

AJCC: American Joint Committee on Cancer

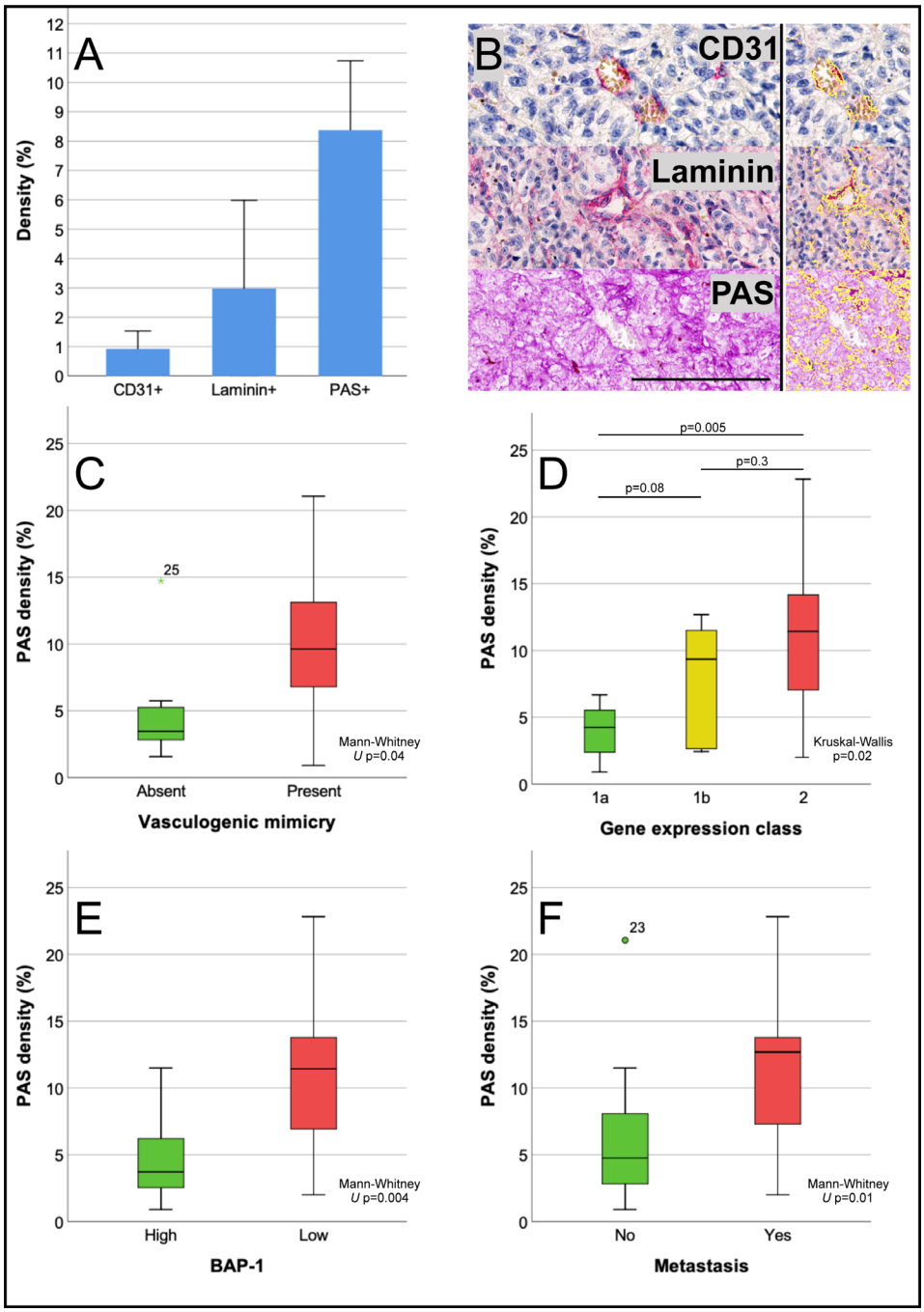

Figure 2. Area density of CD31, laminin, and PAS positive patterns in uveal melanoma. **A**: Mean density of each marker, exemplified in **B**, which also illustrates the digital pattern recognition of each marker in this area (right panel, identified structures marked yellow). **C**: Box plot showing periodic acid-Schiff (PAS) density (PAS positive pixels divided by the total number of pixels) versus the presence (red) or no presence (green) of vasculogenic mimicry, defined as networks, closed loops, or arcs with branching, or any combination (Mann–Whitney *U* test p=0.04). **D**: PAS density versus gene expression class 1a (green), 1b (yellow), or 2 (red; Kruskal–Wallis p=0.02). **E**: PAS density versus level of BAP-1 expression high (green) or low (red) in tumor cell nuclei (Mann–Whitney *U* test p=0.004). **F**: PAS density versus no metastasis (green) or metastasis (red; Mann–Whitney *U* test p=0.01). Error bars represent 95% confidence interval. °=outlier, *=extreme outlier. Scale bar: 100 µm.

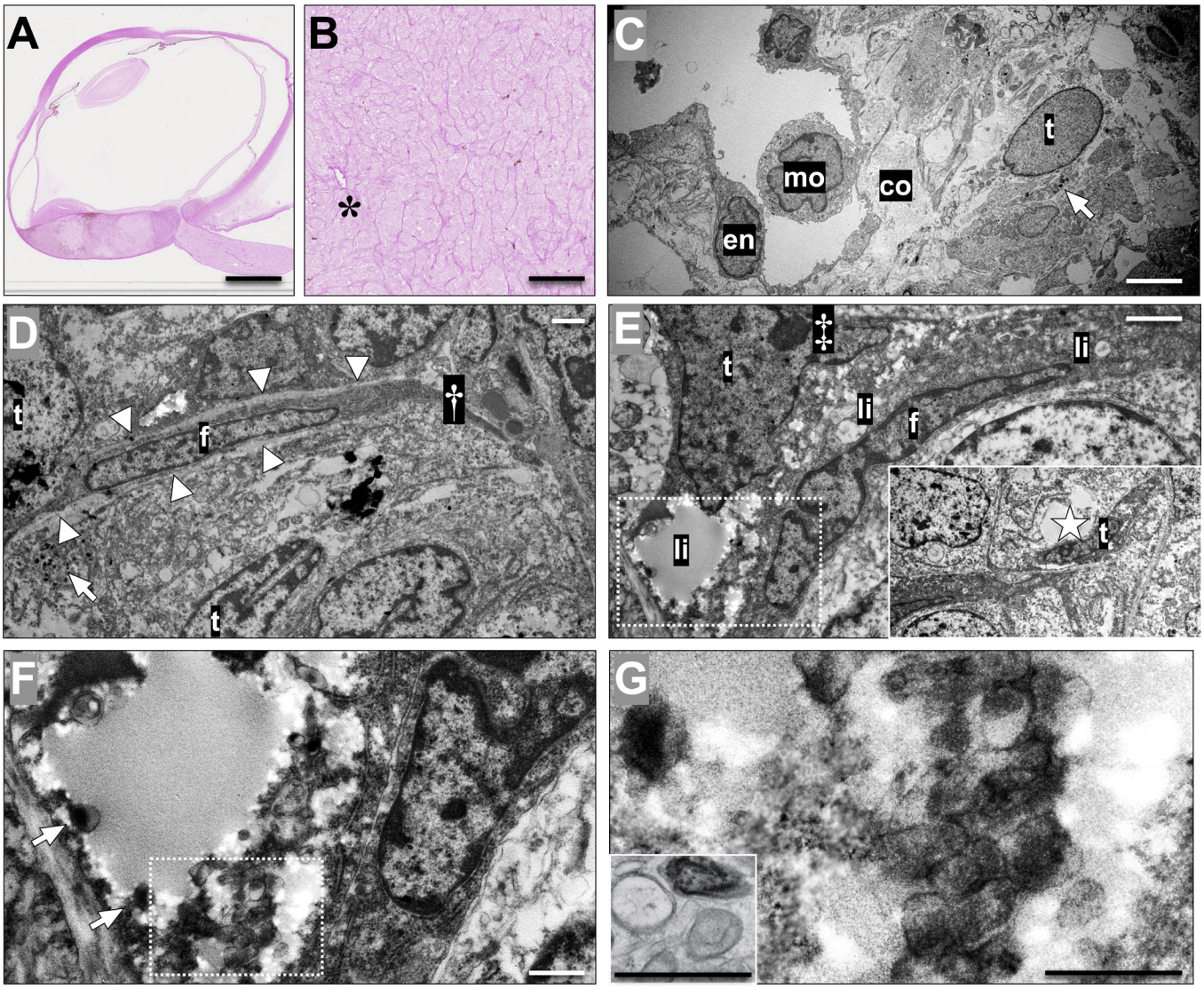

Figure 3. Choroidal vessels and vasculogenic mimicry with bright-field microscopy and transmission electron microscopy. **A**: Tissue section from an enucleated eye with a posterior choroidal melanoma, stained with periodic acid-Schiff (PAS) without hematoxylin counterstain. **B**: In higher magnification, patterns of vasculogenic mimicry including closed loops and networks surrounding packets of melanoma cells can be identified, along with a blood vessel (asterisk). **C**: In transmission electron microscopy of the same tumor, a blood vessel can be identified with a lumen containing a monocyte (mo, marking the nucleus) and a lining of endothelium (en). The vessel is surrounded by bundles of collagen (co) and a tumor cell (t) with cytoplasmic melanosomes (arrow). **D**: In another area of the tumor, a fibroblast (f) is wedged between tumor cells (t), the latter being identifiable by cytoplasmic melanosomes (arrow). The fibroblast is associated with a fibrous septum extending outside the cytoplasm (†), and is lined on both sides by a light, thin basal lamina (arrowheads). However, no potential lumen or fluid can be identified in this area. **E**: In contrast, in yet another tumor area, a tumor cell (t), characterized by a large nucleus with a nucleolus (‡), can be seen sharing a potential space full of debris and lipid droplets (li) with a fibroblast (f). No basal lamina can be identified between the fibroblast and the tumor cells. The potential space extends to a larger sinus (insert, sinus marked by a star), which is lined by a flattened tumor cell (t), recognizable by its large nucleolus and coarse chromatin. **F**: Magnification of the area within the dashed box in **E.** Note that melanosomes can be seen in the cytoplasm of the tumor cell (arrows). **G**: Magnification of the area within the box in **F**. Note that in addition to the mature melanosomes, ovoid premalonosomes can be identified (arrowheads), comparable to an example of premature and mature melanosomes in a line of MNT-1 skin melanoma cells, fixed by high-pressure freezing (insert, modified from Raposo et al. [27]; reprinted with permission from Springer Nature). This tumor was classified as 1a by gene expression profiling, and had retained nuclear BAP-1 expression. Still, the patient developed metastases 10 months after enucleation. Scale bars: a: 5 mm. b: 200 µm. c: 5 µm. d, e: 2 µm. f, g: 1 µm.

expression class dichotomized as class 2 (associated with poor prognosis) versus 1a or 1b (associated with better prognosis) and tumor thickness as covariates, the time-dependent hazard for metastasis was statistically significantly increased for patients who had tumors of gene expression class 2 (hazard class 2 versus 1a or 1b=5.1, 95% CI 1.4–19.1, p=0.02). PAS density was statistically significantly greater in tumors of gene expression class 2, when gene expression class was dichotomized (1 versus 2, Mann–Whitney *U* test p=0.007) and three-tiered (1a versus 1b versus 2, Kruskal–Wallis p=0.02, Figure 2D). Furthermore, a global PAS density greater than the median was associated with gene expression class 2 (Fisher's exact p=0.02). When adjusted for global PAS density, the prognostic significance of gene expression class 2 also disappeared (multiple Cox proportional hazards regression, gene expression class 2 versus 1a or 1b with PAS density less or greater than the median as covariate=1.7, 95% CI 0.3–10.1, p=0.6).

PAS density versus BAP-1 expression: By manual assessment of the level of nuclear BAP-1 expression, 12 tumors were classified as high (normal) and 20 as low (mutated). In a multiple Cox proportional hazards regression with the tumors' nuclear BAP-1 expression and tumor thickness as covariates, the time-dependent hazard for metastasis was borderline statistically significantly increased for patients who had tumors with low BAP-1 expression (hazard low versus high BAP-1 expression=6.8, 95% CI 0.9–53.0, p=0.06). PAS density was statistically significantly higher in tumors with low BAP-1 expression (Mann–Whitney *U* test p=0.004, Figure 2E). Further, a global PAS density greater than the median was associated with low BAP-1 expression (Fisher's exact p=0.02). When adjusted for global PAS density, the borderline prognostic significance of BAP-1 expression disappeared (multiple Cox proportional hazards regression, BAP-1 expression low versus high with PAS density greater or less than the median as covariate=2.1, 95% CI 0.2–21.6, p=0.5).

Vasculogenic mimicry versus BAP-1 expression: The time-dependent and size-adjusted hazard for metastasis was statistically significantly increased for tumors with the presence of networks, closed loops, or arcs with branching, or any combination (hazard pattern versus no pattern=9.6, 95% CI 1.2–77.9, p=0.03). These patterns of VM could be identified in a statistically significantly higher proportion of tumors with low BAP-1 expression (present in 13 tumors with low and in four tumors with high nuclear BAP-1 expression, absent in four tumors with low and seven tumors with high nuclear BAP-1 expression, Fisher's exact p=0.05). The likelihood ratio for the presence of any of these patterns with each decreased step in the four grades of BAP-1 expression was 8.1 (p=0.04).

Metastasis-free survival and logistic regressions: PAS density was statistically significantly higher in tumors that metastasized (Mann–Whitney *U* test p=0.01, Figure 2E). The cumulative 5-year Kaplan–Meier metastasis-free survival decreased for each quartile of increased PAS density (1.0, 0.75, 0.40, and 0.17 for the four quartiles from lowest to highest density, log rank p for trend=0.004) and for a PAS density greater than the median (0.65 versus 1.0, log rank p=0.005, Figure 4A). Similarly, metastasis-free survival was statistically significantly worse for patients with tumors that displayed VM, had low nuclear BAP-1 expression, and were of gene expression class 2 (Figure 4B–D).

In bivariate logistic regression, the presence of networks, closed loops, or arcs with branching, or any combination (odds ratio=18.3, p=0.01), gene expression class (odds ratio for each increased step from 1a to 1b to 2=5.4, p=0.01, for class 2 versus 1a or 1b=12.8, p=0.03), low BAP-1 expression (odds ratio=20.4, p=0.01), and global PAS density (odds ratio for each quartile of increased density 3.6, p=0.01, for greater versus less than median=12.4, p=0.01), but not the density of CD31 or laminin positive pixels, were all individually associated with metastasis (Table 2).

In multiple logistic regression including all six of these variables, none retained statistical significance (p=0.3–0.9). If only the presence of VM and PAS density were included, statistical significance was still not retained (p=0.2–0.3).

Intratumor region analysis: When the tumors were subdivided into circular 2.0 mm diameter sections, a mean of 8.5 (SD 1.2) intratumor regions per tumor were obtained, corresponding to a total of 212 regions across all 28 tumors. One hundred fourteen of these regions (54%) had high BAP-1 expression, and 98 (46%) had low BAP-1 expression. There was VM present in 69 of the regions (32%). In tumors that had any presence of VM, it was seen in an average of 3.2 regions (SD 2.5), corresponding to an area of 10 mm^2. Eleven out of 28 tumors (40%) had heterogeneous BAP-1 expression in the sense that they had at least one region with high BAP-1 expression when the rest of the regions in that tumor had low BAP-1 expression, or vice versa (BAP-1 heterogeneity). Tumors with BAP-1 heterogeneity had worse metastasis-free survival (log rank p=0.03). Tumors with gene expression class 2 were not more likely to display BAP-1 heterogeneity (Fisher's exact p=0.6), but were more likely to contain at least one region with VM (networks, closed loops, or arcs with branching, or any combination, Fisher's exact p=0.03). Regions with low BAP-1 expression were more likely to harbor VM (Fisher's exact p<0.0001), and had a mean PAS

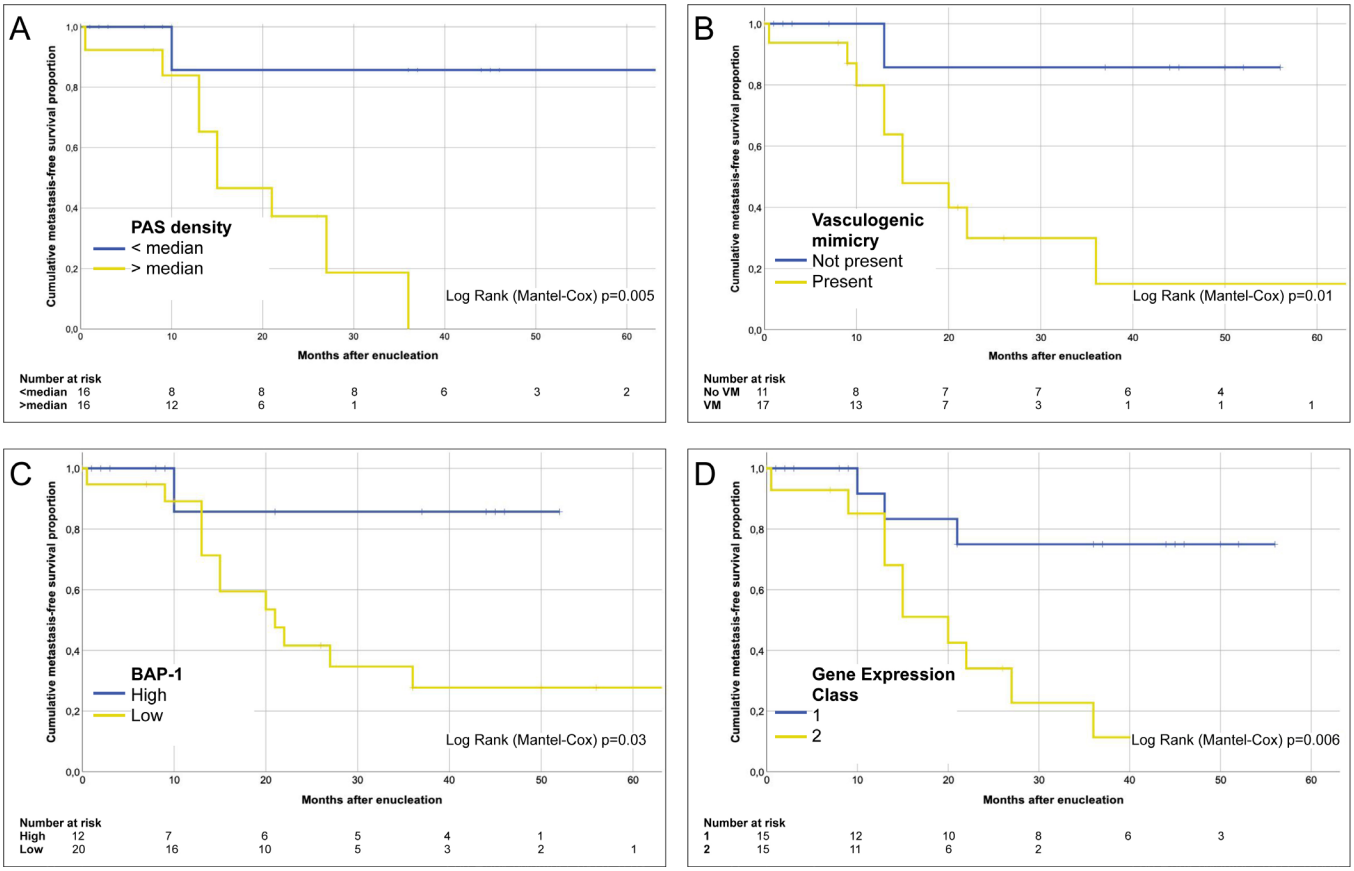

Figure 4. Kaplan–Meier cumulative metastasis-free survival proportion after enucleation. **A**: For patients with tumors that had a periodic acid-Schiff (PAS) density greater than the median, median survival was 15 months (95% confidence interval [CI] 7.0–23; 6.9%). Median survival was not met for tumors that had a PAS density below the median (log rank (Mantel-Cox) p=0.005). **B**: For patients with tumors that displayed vasculogenic mimicry (defined as the presence of networks, closed loops, or arcs with branching, or any combination), median survival was 15 months (95% CI 7.0–23). Median survival was not met for tumors without vasculogenic mimicry (log rank (Mantel-Cox) p=0.01). **C**: For patients with tumors that had low nuclear BAP-1 expression, median survival was 21 months (95% CI 12–30). Median survival was not met for tumors with high nuclear BAP-1 expression (log rank (Mantel-Cox) p=0.03). **D**: For patients with tumors of gene expression class 2, median survival was 20 months (95% CI 12–28). Median survival was not met for tumors with gene expression classes 1a or 1b (log rank (Mantel-Cox) p=0.006).

Table 2. Bivariate logistic regression for association with metastasis.

Bivariate logistic regression	Regression coefficient, β (SE)	Wald statistic	P	Odds ratio, Exp(β; 95% CI)
Bivariate logistic regression				
Vasculogenic mimicry*	2.9 (1.2)	6.2	0.01	18.3 (1.9–179.9)
Gene expression class†	2.6 (0.9)	8.7	<0.01	12.8 (2.4–69.7)
BAP-1 expression	3.0 (1.1)	6.9	0.01	20.4 (2.2–192.6)
PAS density	2.5 (1.0)	6.7	0.01	12.4 (1.8–83.8)
CD31 density	1.5 (1.7)	0.8	0.38	4.3 (0.2–114)
Laminin density	1.8 (1.7)	1.2	0.28	6.1 (0.2–168)

*Vasculogenic mimicry defined as the presence of networks, closed loops or arcs with branching, or any combination thereof. † Gene expression class dichotomized as 2 versus 1a or 1b. PAS: Periodic acid-Schiff

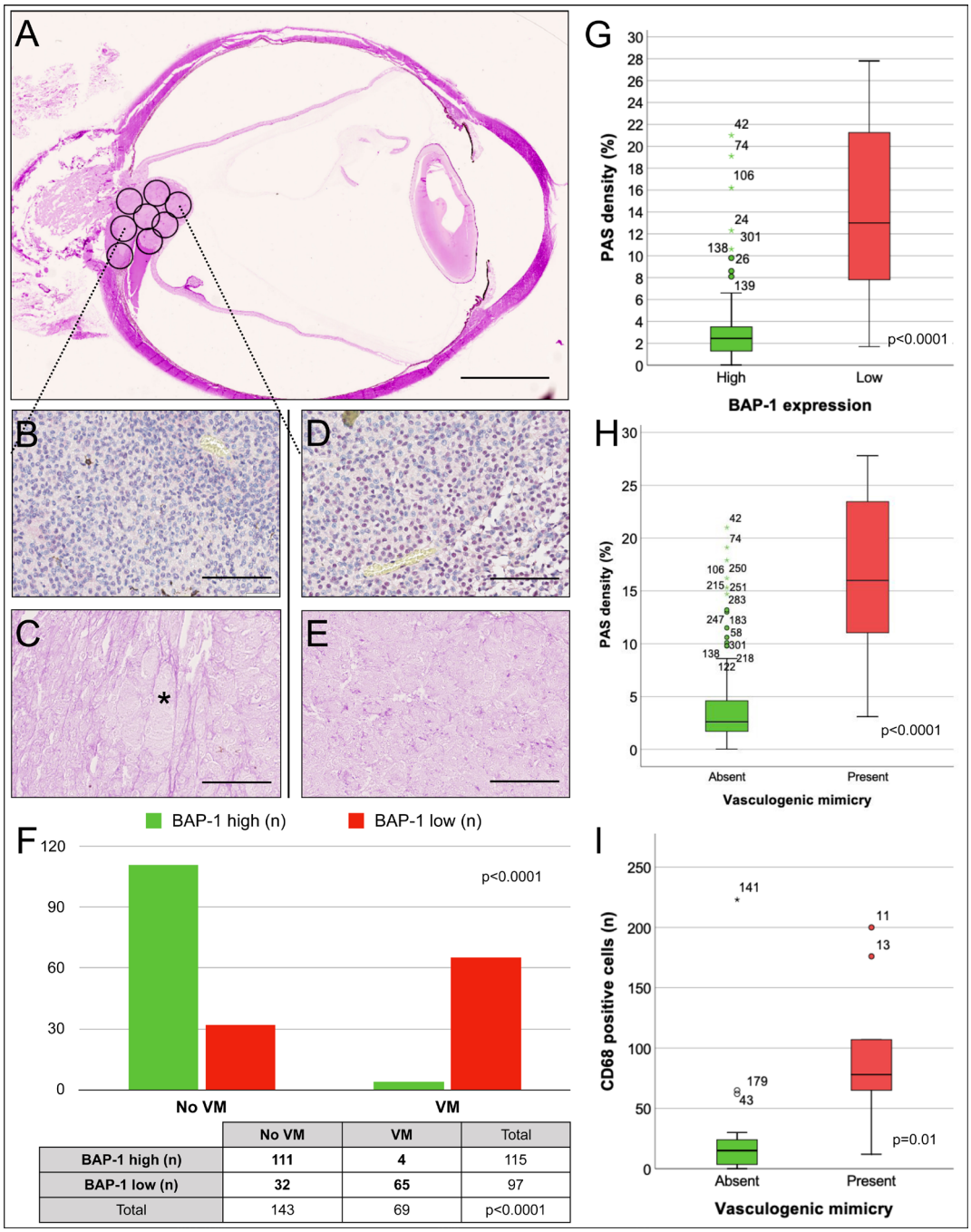

	No VM	VM	Total
BAP-1 high (n)	**111**	**4**	115
BAP-1 low (n)	**32**	**65**	97
Total	143	69	p<0.0001

Figure 5. Intratumor heterogeneity analysis. **A**: Tumors were subdivided into circular 2.0 mm diameter sections for analysis of differences in BAP-1 expression, PAS density, and presence of VM on an intratumor region level. In this example, a region at the base of a tumor (b and c) is compared to a region at the apex of the tumor **(D** and **E**). **B**: In the former, BAP-1 expression can be seen in approximately 30% of tumor cell nuclei. **C**: In the periodic acid-Schiff (PAS) stain from the corresponding tumor region, patterns of vasculogenic mimicry (VM) are identifiable, including a closed loop (asterisk). **D**: In the region at the apex of the tumor, BAP-1 expression is higher. **E**: No patterns of VM can be seen. **F**: Bar plot and cross tabulation comparing BAP-1 expression and the presence of VM in 212 intratumor regions. Regions with low BAP-1 expression correlated to regions with VM and vice versa (Fisher's exact p<0.0001). **G**: Box plot showing PAS density in intratumor regions with low versus high BAP-1 expression (Mann–Whitney *U* test p<0.0001). **H**: Box plot showing PAS density in intratumor regions with and without VM (Mann–Whitney *U* test p<0.0001). **I**: Box plot showing the number of CD68 positive cells in regions with and without VM (Mann–Whitney *U* test p=0.01). Error bars represent 95% confidence interval. °=outliers, *=extreme outliers. Outlier number identifying consecutive intratumor region 1–212. Scale bars: a: 5 mm. b to e: 100 µm.

density of 13.4%, which was statistically significantly greater than the mean PAS density of 3.4% in regions with high BAP-1 expression (Mann–Whitney *U* p<0.0001). Regions with low BAP-1 expression also harbored a statistically significantly higher number of CD68 positive macrophages (Mann–Whitney *U* test p=0.02).

Regions with the presence of VM had a mean PAS density of 16.9%, which was statistically significantly greater than the mean PAS density of 4.2% in regions without VM (Mann–Whitney *U* p<0.0001). Regions with the presence of VM also had a statistically significantly higher number of CD68 positive macrophages (Mann–Whitney *U* test p=0.01, Figure 5).

When the tumors were further subdivided into circular 0.5 mm diameter sections, the mean density of the PAS positive structures in the least dense sections was 3.1% (SD 3.7) and in the densest sections 15.4% (SD 9.4), with the mean difference between the two being 12.3 percentage points (SD 7.4). Closest to the tumors' scleral base, the mean density of the PAS positive structures was 7.0% (SD 6.0). In the tumors' central regions, it was 4.4% (SD 5.0, Mann–Whitney *U* test base-center p=0.1), and at the tumor apexes just beneath Bruch's membrane 5.8% (SD 5.5, Mann–Whitney *U* test base-apex p=0.5, center-apex p=0.2).

DISCUSSION

In this study, we showed the prognostic utility of PAS density in UM, and related it to established markers of prognosis, including gene expression class, nuclear BAP-1 expression, and presence of vasculogenic mimicry. Furthermore, the observations indicated that PAS positive ECM is not only a prognostic marker but also crucial for understanding how UM metastasizes. Based on the findings that a statistically significant proportion of the PAS positive patterns is negative for markers of the endothelium and basal laminae, that the density of CD31 and laminin positive structures is not individually associated with metastasis, that the prognostic significance of VM disappears when adjusting for the density of any type of PAS positive structure within a tumor, and the observations in transmission electron microscopy of tumor cells, fibroblasts, and macrophages in relation to dense strands of ECM, extracellular debris, and VM, we believe that the area density of the ECM, secreted and modified in interplay between these cells, is highly important for increasing the risk for metastasis. The significance of this interaction between the tumor cells and the ocular microenvironment for promotion of aggressive disease might be inferred from previous experiments by Yang et al. [29], in which mice developed statistically significantly more hepatic micrometastases after injection of UM cell lines in the posterior compartment of the eye than after injection in the tail vein. The development of metastasis is a complex multistep process in which tumor cells acquire the ability to detach from the primary site, interact with the ECM and immune system, invade through basal laminae and endothelium, survive in the circulation, implant at the distant site, and subsequently, proliferate [30]. We proposed that in UM, interactions with the ECM and the immune system are key events in this cascade. If injected directly into the systemic circulation, UM cells have no opportunity to undergo selection based on such interactions, and consequently, have less chance of survival. Further, we showed that PAS density is also associated with gene expression class and BAP-1 expression, both of which are highly relevant for prediction of metastases.

The findings on the intertumor level were essentially repeated on the intratumor level. Regions with low BAP-1 expression was statistically significantly more likely to harbor VM, and have statistically significantly greater PAS density and number of CD68 positive cells. Intratumor regions do not merely mirror the status of the parent tumor, e.g., 40% of the tumors had heterogenic expression of BAP-1, and patients with these tumors had statistically significantly worse survival. The presence of BAP-1 heterogeneity is in accordance with one of our previous publications, in which the mean proportion of BAP-1 positive cells was 43.9%, indicating that UMs do not consist of a clone of cells with homogenous BAP-1 expression [31].

We hypothesized that PAS density may be but a marker for a driver behind metastatic behavior. Hypoxic conditions are known to foster tumor cell invasiveness and secretion of vascular endothelial growth factors (VEGFs) [32,33]. As shown by Yang et al., UM expresses VEGF, which suppression inhibits the formation of vascular tubules in vitro and the growth of primary tumors and the formation of hepatic micrometastases in vivo [34]. Consequently, a high PAS density may be the result of a hypoxic behavior, which has made intratumor regions with low BAP-1 expression more invasive. In accordance with a previous publication by Folberg et al. [35], in which the number of foci with VM was higher in the peripheral zones of UM, we found that the PAS density was higher close to the tumors' apexes and scleral bases than in their central regions. Following the logic of our own hypothesis, this would suggest that the peripheral regions of UM are more hypoxic, which would not quite fit the pattern of heterogeneous distribution of pO_2 values seen in several other tumors [36]. We use the term hypoxic behavior because we cannot exclude that this switch to a hypoxic phenotype can occur under normoxia, or as a prolonged response to transient

hypoxia, similar to the Warburg effect of aerobic glycolysis [37]. Although mutations in *BAP-1* (Gene ID 8314, OMIM 603089) have been described as random events [38], we do not know if there is a behavioral difference in response to hypoxia between BAP-1 mutants and a residual population of BAP-1 wild-type tumor cells. We sought to clarify this in an ongoing investigation.

This study had several limitations. First, the results were based on a small retrospective cohort that just met the minimum sample size in the power calculation. The previous study we based the cohort size on also had access to a longer follow-up, limiting the validity of the size assumption. Ideally, we would have had multiple tumor sections from each tumor to better account for intratumor heterogeneity. Second, although the automatic detection of PAS density presented here offers a relatively fast and simple alternative to previous methods based on manual assessments of immunohistochemical stains, it is in our opinion still not fast or simple enough for application in everyday clinical practice. Intra- or interobserver variability in determinations of PAS density was not studied. Third, as reported by Chen et al. [39] and Pisacane et al. [40], melanoma cells may express endothelial markers CD34 and CD31. Similarly, melanoma cells with certain differentiations have been noted to contain intracytoplasmic glycogen and be PAS positive [41,42]. Therefore, we used the term PAS density to denote the area density of any PAS positive pixel within the tumors, without any further exclusions based on anatomic structures, organelles, or other properties. Nevertheless, the reader should be aware that the true densities of endothelium and PAS positive extracellular patterns may be lower than reported here. Fourth, the inferences drawn from transmission electron microscopy should be interpreted with caution, as there was limited sampling for this analysis.

In conclusion, we found that the strong association between VM and metastasis of UM disappears when corrected for the density of any PAS positive pattern, including blood vessels and basal laminae. On the intratumor level, regions with low BAP-1 expression were statistically significantly more likely to harbor VM, and have statistically significantly greater PAS density and number of CD68 positive cells. We argue that the area density of the ECM, secreted and modified in interplay between tumor cells, fibroblasts, and macrophages, is highly important for increasing the risk for metastasis.

ACKNOWLEDGMENTS

Funding: Support for this study was provided to Gustav Stålhammar from St. Erik Eye Hospital, the St. Erik Research Foundation (S:t Eriks Ögonforskningsstiftelse), the Swedish Ophthalmological Society, Cronqvist Foundation (Cronqvists stiftelse), the Swedish Eye Foundation (Ögonfonden) and Karolinska Institutet (Karolinska Institutets stiftelsemedel för ögonforskning) and to Hans E. Grossniklaus from the National Institutes of Health, grant numbers NIH R01CA176001 and NIH P30EY06360 and an unrestricted departmental grant from Research to Prevent Blindness, Inc.

REFERENCES

1. Singh AD, Shields CL, Shields JA. Prognostic factors in uveal melanoma. 2001. p. 806–7.
2. Eschelman DJ, Gonsalves CF, Sato T. Transhepatic therapies for metastatic uveal melanoma. Semin Intervent Radiol 2013; 30:39-[PMID: 24436516].
3. Lane AM, Kim IK, Gragoudas ES. Survival Rates in Patients After Treatment for Metastasis From Uveal Melanoma. JAMA Ophthalmol 2018; 136:981-[PMID: 29955797].
4. Kivelä T, Simpson ER, Grossniklaus HE, Jager MJ, Singh AD, Caminal JM, Pavlick AC, Kujala E, Coupland SE, Finger PT. Uveal Melanoma. AJCC Cancer Staging Manual. 8 ed. Chicago: Springer; 2017. p. 805-17.
5. Fuchs E. Das Sarkom des Uvealtractus. Graefe's Archiv für Ophthalmologie 1882; 12:144-7. .
6. Folberg R, Maniotis AJ. Vasculogenic mimicry. APMIS 2004; 112:508-25. [PMID: 15563313].
7. Maniotis AJ, Folberg R, Hess A, Seftor EA, Gardner LMG. Pe, Amp, Apos, Er J, Trent JM, Meltzer PS, Hendrix MJC. Vascular Channel Formation by Human Melanoma Cells in Vivo and in Vitro: Vasculogenic Mimicry. Am J Pathol 1999; 155:739-52. [PMID: 10487832].
8. Daniels KJ, Boldt HC, Martin JA, Gardner LM, Meyer M, Folberg R. Expression of type VI collagen in uveal melanoma: its role in pattern formation and tumor progression. Lab Invest 1996; 75:55-66. [PMID: 8683940].
9. Seregard S, Spångberg B, Juul C, Oskarsson M. Prognostic accuracy of the mean of the largest nucleoli, vascular patterns, and PC-10 in posterior uveal melanoma. Ophthalmology 1998; 105:485-91. [PMID: 9499780].
10. McLean IW, Keefe KS, Burnier MN. Uveal melanoma. Comparison of the prognostic value of fibrovascular loops, mean of the ten largest nucleoli, cell type, and tumor size. Ophthalmology 1997; 104:777-80. [PMID: 9160022].
11. Folberg R, Pe'Er J, Gruman LM, Woolson RF, Jeng G, Montague PR, Moninger TO, Yi H, Moore KC, Montague PR, Moninger TO, Yi H, Moore KC. The morphologic characteristics of tumor blood vessels as a marker of tumor progression in primary human uveal melanoma: A matched

case-control study. Hum Pathol 1992; 23:1298-305. [PMID: 1427757].

12. Onken MD, Lin AY, Worley LA, Folberg R, Harbour JW. Association Between Microarray Gene Expression Signature and Extravascular Matrix Patterns in Primary Uveal Melanomas. Am J Ophthalmol 2005; 140:748-9. [PMID: 16226537].

13. Mäkitie T, Summanen P, Tarkkanen A, Kivelä T. Microvascular density in predicting survival of patients with choroidal and ciliary body melanoma. Invest Ophthalmol Vis Sci 1999; 40:2471-[PMID: 10509639].

14. Foss AJE, Alexander RA, Hungerford JL, Harris AL, Cree IA, Lightman S. Reassessment of the PAS patterns in uveal melanoma. Br J Ophthalmol 1997; 81:240-[PMID: 9135390].

15. Lin YA, Ai JZ, Lee JS-C, Bajcsy JP. Pe'er JJ, Leach JL, Maniotis JA, Folberg JR. Comparing Vasculogenic Mimicry With Endothelial Cell-lined Vessels: Techniques for 3D Reconstruction and Quantitative Analysis of Tissue Components from Archival Paraffin Blocks. Appl Immunohistochem Mol Morphol 2007; 15:113-9. [PMID: 17536318].

16. Foss AJ, Alexander RA, Jefferies LW, Hungerford JL, Harris AL, Lightman S. Microvessel count predicts survival in uveal melanoma. Cancer Res 1996; 56:2900-[PMID: 8674036].

17. Piña Y, Cebulla CM, Murray TG, Alegret A, Dubovy SR, Boutrid H, Feuer W, Mutapcic L, Jockovich M-E. Blood Vessel Maturation in Human Uveal Melanoma: Spatial Distribution of Neovessels and Mature Vasculature. Ophthalmic Res 2009; 41:160-9. [PMID: 19321938].

18. Mäkitie T, Summanen P, Tarkkanen A, Kivelä T. Tumor-infiltrating macrophages (CD68(+) cells) and prognosis in malignant uveal melanoma. Invest Ophthalmol Vis Sci 2001; 42:1414-[PMID: 11381040].

19. Herwig MC, Bergstrom C, Wells JR, Höller T, Grossniklaus HE. M2/ M1 ratio of tumor associated macrophages and PPAR- gamma expression in uveal melanomas with class 1 and class 2 molecular profiles. Exp Eye Res 2013; 107:52-8. [PMID: 23206928].

20. Szalai E, Wells JR, Ward L, Grossniklaus HE. Uveal Melanoma Nuclear BRCA1-Associated Protein-1 Immunoreactivity Is an Indicator of Metastasis. Ophthalmology 2018; 125:203-9. [PMID: 28823399].

21. Kalirai H, Dodson A, Faqir S, Damato BE, Coupland SE. Lack of BAP1 protein expression in uveal melanoma is associated with increased metastatic risk and has utility in routine prognostic testing. Br J Cancer 2014; 111:1373-1380. [PMID: 25058347].

22. Gezgin G, Dogrusöz M, Essen T, Kroes W, Luyten G, Velden P, Walter V, Verdijk R, Hall T, Burg S, Jager M. Genetic evolution of uveal melanoma guides the development of an inflammatory microenvironment. Cancer Immunol Immunother 2017; 66:903-12. [PMID: 28391358].

23. Van De Nes APJ, Nelles HDJ, Kreis RS, Metz RC, Hager RT, Lohmann RD, Zeschnigk RM. Comparing the Prognostic Value of BAP1 Mutation Pattern, Chromosome 3 Status, and BAP1 Immunohistochemistry in Uveal Melanoma. Am J Surg Pathol 2016; 40:796-805. [PMID: 27015033].

24. Bankhead P, Loughrey M, Fernández J, Dombrowski Y, McArt D, Dunne P, McQuaid S, Gray R, Murray L, Coleman H, James J, Salto-Tellez M, Hamilton P. QuPath: Open source software for digital pathology image analysis. Sci Rep 2017; 7:16878-[PMID: 29203879].

25. Onken MD, Worley LA, Tuscan MD, Harbour JW. An Accurate, Clinically Feasible Multi-Gene Expression Assay for Predicting Metastasis in Uveal Melanoma. J Mol Diagn 2010; 12:461-8. [PMID: 20413675].

26. Onken MD, Worley LA, Char DH, Augsburger JJ, Correa ZM, Nudleman E, Aaberg TM, Altaweel MM, Bardenstein DS, Finger PT, Gallie BL, Harocopos GJ, Hovland PG, McGowan HD, Milman T, Mruthyunjaya P, Simpson ER, Smith ME, Wilson DJ, Wirostko WJ, Harbour JW. Collaborative Ocular Oncology Group report number 1: prospective validation of a multi-gene prognostic assay in uveal melanoma. Ophthalmology 2012; 119:1596-603. [PMID: 22521086].

27. Raposo G, Marks MS. Melanosomes–dark organelles enlighten endosomal membrane transport. Nat Rev Mol Cell Biol 2007; 8:786-[PMID: 17878918].

28. Arnljots TS, Al-Sharbaty Z, Lardner E, All-Eriksson C, Seregard S, Stålhammar G. Tumour thickness, diameter, area or volume? The prognostic significance of conventional versus digital image analysis-based size estimation methods in uveal melanoma. Acta Ophthalmol 2018; 96:510-8. [PMID: 29338132].

29. Yang EH, Fang EG, Huang EX, Yu EJ, Hsieh EC-L, Grossniklaus EH. In-vivo xenograft murine human uveal melanoma model develops hepatic micrometastases. Melanoma Res 2008; 18:95-103. [PMID: 18337645].

30. Klaus P, Ruud HB. Dissecting the metastatic cascade. Nat Rev Cancer 2004; 4:448-[PMID: 15170447].

31. Stålhammar G, See TRO, Phillips S, Seregard S, Grossniklaus HE. Digital Image Analysis of BAP-1 Accurately Predicts Uveal Melanoma Metastasis. Transl Vis Sci Technol 2019; 8:11-[PMID: 31110912].

32. Hu K, Babapoor-Farrokhran S, Rodrigues M, Deshpande M, Puchner B, Kashiwabuchi F, Hassan SJ, Asnaghi L, Handa JT, Merbs S, Eberhart CG, Semenza GL, Montaner S, Sodhi A. Hypoxia-inducible factor 1 upregulation of both VEGF and ANGPTL4 is required to promote the angiogenic phenotype in uveal melanoma. Oncotarget 2016; 7:7816-28. [PMID: 26761211].

33. Laura A, Michael HL, Kah Suan L, Kah Jing L, Arushi T, Murilo W, Shannath LM, James TH, Akrit S, Eli EB, Charles GE. Hypoxia promotes uveal melanoma invasion through enhanced Notch and MAPK activation. PLoS One 2014; 9:e105372-[PMID: 25166211].

34. Yang H, Jager MJ, Grossniklaus HE. Bevacizumab suppression of establishment of micrometastases in experimental ocular melanoma. Invest Ophthalmol Vis Sci 2010; 51:2835-42. [PMID: 20089875].

35. Folberg R, Fleck M, Mehaffey MG, Meyer M, Bentler SE, Woolson RF, Pe'er J. Mapping the Location of Prognostically Significant Microcirculatory Patterns in Ciliary Body and Choroidal Melanomas. Pathol Oncol Res 1996; 2:229-36. [PMID: 11173608].

36. Vaupel P, Mayer A. Hypoxia in cancer: significance and impact on clinical outcome. Cancer Metastasis Rev 2007; 26:225-39. [PMID: 17440684].

37. Vander Heiden MG, Cantley LC, Thompson CB. Understanding the Warburg effect: the metabolic requirements of cell proliferation. Science 2009; 324:1029-[PMID: 19460998].

38. Szalai E, Jiang Y, van Poppelen NM, Jager MJ, de Klein A, Kilic E, Grossniklaus HE. Association of Uveal Melanoma Metastatic Rate With Stochastic Mutation Rate and Type of Mutation. JAMA Ophthalmol 2018; 136:1115-[PMID: 30073324].

39. Chen X, Maniotis AJ, Majumdar D, Pe'Er J, Folberg R. Uveal melanoma cell staining for CD34 and assessment of tumor vascularity. Invest Ophthalmol Vis Sci 2002; 43:2533-[PMID: 12147581].

40. Pisacane A, Picciotto F, Risio M. CD31 and CD34 Expression as Immunohistochemical Markers of Endothelial Transdifferentiation in Human Cutaneous Melanoma. Cell Oncol 2007; 29:59-66. [PMID: 17429142].

41. Nowak MA, Fatteh SM, Campbell TE. Glycogen-rich malignant melanomas and glycogen-rich balloon cell malignant melanomas: frequency and pattern of PAS positivity in primary and metastatic melanomas. Arch Pathol Lab Med 1998; 122:353-60. [PMID: 9648905].

42. Grossniklaus HE, Albert DM, Green WR, Conway BP, Hovland KR. Clear cell differentiation in choroidal melanoma. COMS report no. 8. Collaborative Ocular Melanoma Study Group. Arch Ophthalmol 1997; 115:894-8. [PMID: 9230830].

Articles are provided courtesy of Emory University and the Zhongshan Ophthalmic Center, Sun Yat-sen University, P.R. China. The print version of this article was created on 21 September 2019. This reflects all typographical corrections and errata to the article through that date. Details of any changes may be found in the online version of the article.